

# Discovery of a New X-ray Filled Radio Supernova Remnant Around the Pulsar Wind Nebula in 3EG J1809–2328

Mallory S.E. Roberts  
Eureka Scientific, Inc., Oakland, CA, USA  
malloryr@gmail.com  
and

Crystal L. Brogan  
National Radio Astronomy Observatory, 520 Edgemont Rd, Charlottesville, VA 22903, USA

## ABSTRACT

We report the discovery of a partial  $\sim 2^\circ$  diameter non-thermal radio shell coincident with Taz, the pulsar wind nebula (PWN) in the error box of the apparently variable  $\gamma$ -ray source 3EG J1809–2328. We propose that this radio shell is a newly identified supernova remnant (SNR G7.5–1.7) associated with the PWN. The SNR surrounds an amorphous region of thermal X-rays detected in archival *ROSAT* and *ASCA* observations putting this system in the mixed-morphology class of supernova remnants. G7.5–1.7 is the fifth such supernova remnant coincident with a bright GeV source, and the fourth containing a pulsar wind nebulae.

*Subject headings:* gamma rays: observations — supernova remnants — pulsars: individual(Taz) — radio continuum: ISM — X-rays: ISM — ISM: individual(G7.5–1.7)

## 1. Introduction

The possibility of supernova remnants (SNRs) being sources of observable GeV emission has long been suggested by theoretical models of cosmic-ray acceleration (see Baring et al. 1999, and references therein) in SNR shocks and by statistical associations with cataloged  $\gamma$ -ray sources (Sturmer & Dermer 1995; Esposito et al. 1996; Yadigaroglu & Romani 1997). However, the direct linking of a particular SNR with a specific  $\gamma$ -ray source detected by the *EGRET* instrument on board the Compton Gamma-Ray Observatory has been elusive (Doherty et al. 2003; Torres et al. 2003) (note we only refer to the results of the supernova blast as SNR, not isolated pulsar wind nebulae (PWN) which are sometimes referred to as “plerionic” or “Crab-like” SNR). The *EGRET* sources with the smallest and most robust error boxes are not positionally coincident with regions of SNRs which show direct evidence of high-energy

particle acceleration through synchrotron emission of X-rays. Although there are five previously known radio SNRs that contain within their shells unidentified *EGRET* sources which are bright above 1 GeV (as defined by Lamb & Macomb 1997), in no case can hard X-ray emission from the SNR blast wave be convincingly associated with the  $\gamma$ -ray source (Roberts et al. 2001a, hereafter, RRK).

Interestingly, four of these SNRs are of the subclass of mixed-morphology SNR (SNR Rho & Petre 1998) which have centrally concentrated thermal X-ray emission within a radio shell. Three of these (CTA 1, IC 443, and W44) also contain young, energetic pulsars which are actively producing high-energy particles as evidenced by their wind nebulae (Brazier et al. 1998; Halpern et al. 2004; Olbert et al. 2001; Harrus et al. 1996). It is therefore unclear as to whether the GeV emission is produced at the SNR forward shock, the interior where the thermal X-ray emission comes from, or

has to do with the pulsar or its wind.

While the source of GeV emission remains unclear, at TeV energies a growing number of sources coincident with PWN and young shell SNR have been discovered by H.E.S.S. (Aharonian et al. 2006c). Several of the TeV emitting PWN are associated with *EGRET* sources, notably the Crab (Weekes et al. 1989), Vela (Aharonian et al. 2006a), and the two nebulae in the Kookaburra radio complex (Aharonian et al. 2006b). Two clear detections of shell SNRs with H.E.S.S. have also been reported (Funk 2006). In these cases, the TeV emission has been shown to be associated with regions of non-thermal X-rays in the shell. A few H.E.S.S. sources coincident with composite SNR have been reported as well (Aharonian et al. 2005; Brogan et al. 2005; Helfand et al. 2007), but in these cases the TeV emission appears to be associated with non-thermal X-rays from the central PWN, not the shell. Two of the mixed-morphology SNR associated with bright GeV sources, IC443 and W28, have recently been detected as sources of TeV emission, but it is unclear what, if any, connection there is between the GeV source and the TeV source (Albert et al. 2007; H. E. S. S. Collaboration: G. Rowell et al. 2007).

Here we report the detection of a non-thermal radio shell with the Very Large Array (VLA) at 90 cm surrounding the PWN associated with the *EGRET* source GeV J1809–2327/3EG J1809–2328. Archival *ROSAT* (Trümper 1982) and *ASCA* (Tanaka et al. 1994) data show a region of diffuse thermal X-ray emission between the radio shell and the PWN suggesting this source is a new mixed-morphology SNR.

## 2. Analysis of Archival X-ray Data in the Region surrounding the Taz PWN

3EG J1809–2328 is one of the brightest sources of  $> 1$  GeV emission in the Galaxy (Hartman et al. 1999; Lamb & Macomb 1997). It has a well determined position (Fig 1) and apparently variable emission above 100 MeV on timescales of months (Nolan et al. 2003). *ASCA* imaging of the *EGRET* error box revealed an extended hard X-ray source (RRK), which (Braje et al. 2002) subsequently resolved into an apparent rapidly-moving PWN (RPWN) and a young stellar cluster using a short *Chandra* observation

(see Kaspi et al. 2006; Gaensler & Slane 2006, for general reviews of PWN). Radio imaging with the VLA and observations with *XMM-Newton* confirm the RPWN nature of the X-ray source (Roberts et al. 2001b; Braje et al. 2002, Roberts et al. in preparation). Due to the radio nebula’s distinctive funnel shape (presumably imposed by its motion), its unusually powerful  $\gamma$ -ray emission, and the growing tradition of naming PWN after animals, this nebula is sometimes referred to as “Taz” (short for tasmanian devil).

The X-ray and radio morphology of Taz, if interpreted as being created by a bowshock, suggests a birthsite to the northwest. A *ROSAT* PSPC exposure corrected 0.1–2.4 keV image obtained through SkyView<sup>1</sup> shows a large region of soft X-ray emission in this direction which we will refer to as G7.5–1.7 (Fig. 1). This inspired a 38 ks observation with the *ASCA* satellite on 1996-09-24 that has not previously been published. Following the imaging and spectral fitting procedures outlined in RRK, we produced combined particle background subtracted, exposure corrected images of the 3EG J1809–2328 and G7.5–1.7 fields from the *ASCA* GIS data in the 0.7–2 keV, 2–10 keV, and 4–10 keV bands (Fig. 2). The higher energy bands show a fairly bright, compact source of hard X-rays in the region of soft thermal X-ray emission which is not evident in the *ROSAT* image. The peak of this source is at RA =  $18^h08^m56.3^s$ , Dec =  $-23^\circ09'57''$  (J2000) in the GIS 2–10 keV image; *ASCA* images have a nominal positional error of  $\sim 24''$  (Gotthelf et al. 2000). We will refer to this hard source as AX J1808.9–2310.

We extracted spectra from two regions in the field of the GIS instruments, one containing the hard source and one containing the soft diffuse emission. Since there is emission essentially throughout the *ASCA* field, we used a background region from the neighboring field which contains the Taz PWN. We fit the soft extended emission to a thermal model, choosing an absorbed *vnei* non-equilibrium model from *XSPEC* to facilitate comparison with other Mixed-Morphology remnants, at first keeping the abundances fixed to solar. To help constrain the soft end of the thermal emission spectrum, we simultaneously fit the

<sup>1</sup>The NASA SkyView Virtual Observatory is located at <http://skyview.gsfc.nasa.gov/>

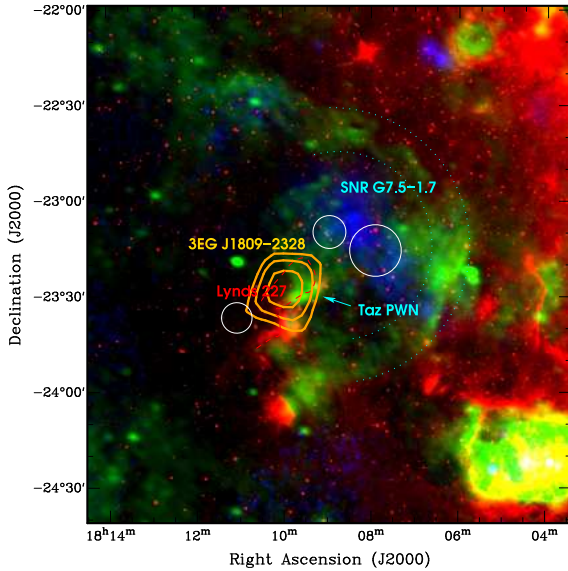


Fig. 1.— Multiwavelength view of G7.5-1.7. MSX 8.3  $\mu\text{m}$  (20'' resolution) is in red, *ROSAT* PSPC 0.1-2.4 keV X-rays (smoothed with an 70'' FWHM Gaussian) are in blue, *VLA* 90 cm radio (168''  $\times$  120'' resolution) is in green. The contours are the 68%, 95% and 99% uncertainty on the position of 3EG J1809-2328. The circles show X-ray spectral extraction regions (see fig. 2). The dotted cyan lines delineate the nominal shell of G7.5-1.7 while the dashed red line shows the approximate outline of the Lynds 227 dark cloud, whose edge is bright in the infrared image. The 90 cm *VLA* image has been corrected for primary beam attenuation.

*ROSAT* PSPC spectrum extracted from the the same region. We obtained an adequate fit using a single temperature with solar abundances. The result is a temperature  $kT = 0.61^{+0.07}_{-0.08}$  keV (90% confidence region), an ionization timescale  $\tau = 1.54^{+0.80}_{-0.47} \times 10^{11} \text{ s cm}^{-3}$  and an absorption  $n_H = 1.5^{+0.8}_{-0.6} \times 10^{21} \text{ cm}^{-2}$ . Note that the *ROSAT* and *ASCA* spectra seemed to differ somewhat near the upper end of the *ROSAT* pass-band ( $\sim 2$  keV) and so these values are somewhat dependent upon which energy bins from *ROSAT* were included in the fits. For example, ignoring the *ROSAT* data above 1.6 keV resulted in an improved chi-squared and a somewhat lower absorption of  $\sim 9 \times 10^{20} \text{ cm}^{-2}$ . Fitting the *ASCA* data by themselves resulted in consistent values, and allowing the abundances to vary did not result in a significantly better fit. We also tried the *ray* and *vray* equilibrium thermal models, but these resulted in statistically inferior fits. The spectral values obtained are typical of temperatures and timescales fit from *ASCA* observations of other mixed-morphology SNR (Kawasaki et al. 2005). Since the thermal X-ray emission covers an area much larger than the field of view of the *ASCA* GIS and it is somewhat unclear what is the total extent even in the *ROSAT* images, an accurate total thermal flux measurement is difficult. However, using the fluxed *ROSAT* maps and extrapolating from our fit spectra, we estimate the total unabsorbed bolometric thermal flux from the remnant to be on the order of  $10^{-10} \text{ erg cm}^{-2} \text{ s}^{-1}$ .

We then fit the hard source (AX J1808.9-2310) to an absorbed power law plus an absorbed *vnei* model, fixing the latter to the values above allowing only the normalization to vary. The result is an absorption  $n_H = 1.9^{+0.5}_{-0.4} \times 10^{22} \text{ cm}^{-2}$ , a spectral index  $\Gamma = 2.57^{+0.29}_{-0.27}$  and a 2-10 keV flux  $F_X = 3.9 \pm 0.1 \times 10^{-12} \text{ ergs cm}^{-2} \text{ s}^{-1}$ . Since there is no evidence for a source of additional foreground absorption in the mid-infrared or optical (see below), the order of magnitude higher absorption toward this source suggests it is an unrelated background object and/or contains significant intrinsic absorption. The total Galactic  $n_H$  in this direction as estimated using the *HEASARC*  $n_H$  tool and the HI maps of Dickey & Lockman (1990) is  $\sim 6 \times 10^{21} \text{ cm}^{-2}$ .

### 3. Radio Observations

We observed the region around Taz at 90 cm with the *VLA* on May 28, 2004 in the DnC configuration (project code AR 547) for 4.5 hours (on-source). We used 32 channels over a bandwidth of 12.6 MHz in LL and RR polarizations. Using AIPS and standard wide-field low frequency imaging techniques (see for example Brogan et al. 2004, and references therein), the resulting image has an effective central observing frequency of 324.84 MHz, an effective bandwidth of 9.38 MHz, a beam size of  $168'' \times 120''$  (P.A. =  $72^\circ$ ) and an RMS level of about 20 mJy/beam. The *VLA* FWHP primary beam at 325 GHz is  $2.5^\circ$ . Due to spatial filtering caused by the missing short spacings, this image is not sensitive to smooth structures larger than  $\sim 1^\circ$ .

The 90 cm image shows a partial shell of emission surrounding the thermal X-ray emission (Fig. 1). Comparison with the  $8.3\mu$  MSX image of the region shows no infrared excess associated with this shell, suggesting a non-thermal origin of the radio emission (Cohen & Green 2001; Brogan et al. 2006). We convolved the 90 cm image with a 2-D Gaussian to produce a  $258''$  resolution image for comparison to the Bonn 11cm Survey image for this region (Reich et al. 1984). We made two spectral index maps from the 90 cm and 11 cm images (assuming  $S_\nu^\alpha$ ), one using the standard 11 cm background subtracted image, and one using an 11 cm image that was passed through a “high-pass” filter in order to mimic the large-scale spatial filtering of the 90 cm *VLA* image. In both spectral index maps, the Taz PWN and the new shell both have significantly steeper spectra than known thermal sources in the region. Overall, the spectral index map created from the filtered 11cm Bonn data (Fig. 3) is steeper, as expected, and provides a better match to the spectra of other known SNR in the field of view. The spectral index of the shell ranges from  $\alpha \sim -0.3$  to  $-0.7$ , with an estimated uncertainty of  $\pm 0.3$  at any particular position. The large uncertainty is dominated by the inherent uncertainty in measuring flux from a large, diffuse object with an interferometer, and not the noise in the images.

The center of the radio shell is at roughly  $l = 7.54^\circ$ ,  $b = -1.90^\circ$  near the northern edge of the Taz radio nebula, and the radius is  $r \sim 0.82^\circ$ .

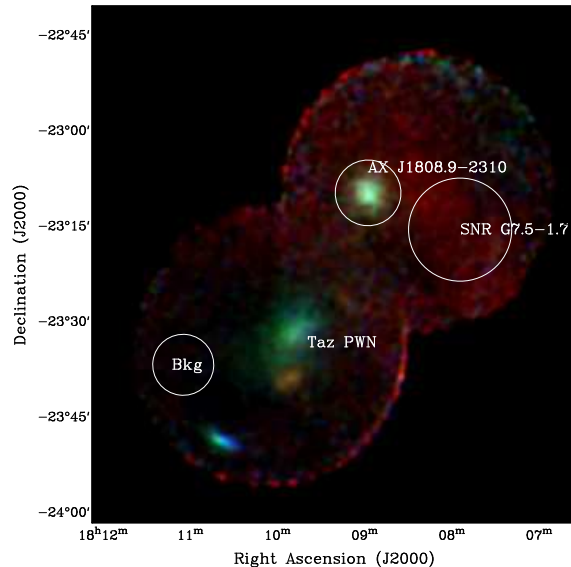


Fig. 2.— *ASCA* GIS X-ray image of G7.5–1.7. Red is 0.7–2 keV, green is 2–10 keV, blue is 4–10 keV ( $\sim 1'$  resolution). The circles show the extraction regions for the X-ray spectral fits of the supernova remnant, the hard source, and the background region.

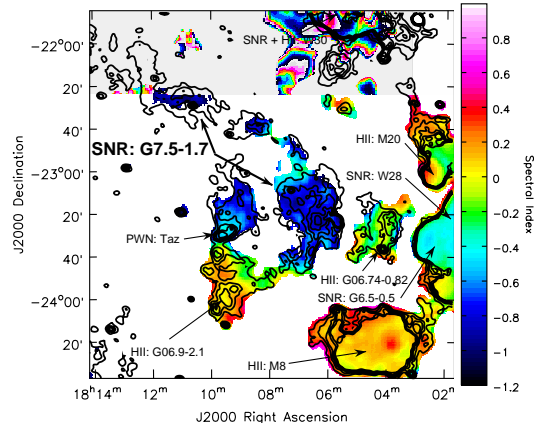


Fig. 3.— Spectral index (assuming  $S_\nu^\alpha$ ) map of G7.5–1.7 and the surrounding region derived from an 11 cm Bonn image and the 90 cm *VLA* image. Before calculating the spectral index, the Bonn image was passed through a “high-pass” filter to mimic the spatial coverage of the *VLA* interferometric data (which are not sensitive to smooth structures larger than  $1^\circ$ ). The 90 cm image was first convolved to the  $258''$  resolution of the Bonn image. The input 11 and 90cm images were masked at 30 and 120 mJy beam $^{-1}$ , respectively. Contours from the  $168'' \times 120''$  resolution 90 cm image are superposed, the contour levels are  $60 \times (1, 2, 3, 4, 5)$  mJy beam $^{-1}$ . Several previously identified HII regions and SNRs are labeled for reference (Griffith et al. 1994; Lockman et al. 1996; Brogan et al. 2006).

The shell has a somewhat smaller radius of curvature ( $r \sim 0.45^\circ$  center at  $l \sim 7.51$ ,  $b \sim -1.42$ ) on the side nearer the Galactic plane, centered in the middle of the thermal X-ray emission. Assuming the origin of the expanding shell lies somewhere in between these two centers and near the symmetry axis of Taz, we will refer to the radio shell as G7.5–1.7.

We have also obtained high resolution ( $3.6'' \times 3.2''$ ) 20 cm *VLA* data of a much smaller field of view centered on the Taz nebula which will be discussed in detail in a future paper that concentrates on the PWN (Roberts et al. in prep.). For the purpose of the present paper it is interesting to note that there is a 13 mJy 20 cm radio source at RA(J2000) =  $18^{\text{h}}08^{\text{m}}57.59^{\text{s}}$ , Dec(J2000) =  $-23^\circ09'45.4''$  that is coincident with the hard *ASCA* source AX J1808.9–2310. The radio source is elongated and well fit by a  $7.4'' \times 1.4''$  Gaussian, suggestive of a barely resolved double jet source.

#### 4. Discussion

G7.5–1.7 has the classic properties of a mixed-morphology supernova remnant (Rho & Petre 1998). The thermal X-ray emission is concentrated between Taz and the Galactic plane side of the radio shell. In both the Bonn 11 cm and our *VLA* 90 cm images, between 1/2 and 3/4 of a radio shell surrounds Taz. The side towards the Galactic plane is brightest, while the side away from the plane is too faint to be sure of any structures, suggesting a strong density gradient in this direction. Comparing to the MSX  $8.3\mu\text{m}$  image, the radio shell is located within a region of low diffuse mid-infrared emission. Numerical models of the evolution of mixed-morphology remnants suggest they are a common stage in the growth of remnants at ages of  $\sim 10,000$ – $100,000$  yr if they are expanding in high-density regions of the ISM (Tilley et al. 2006). In this case where there is an apparent density gradient, the thermal X-ray emission is concentrated near the bright side of the shell, towards the Galactic plane, rather than around the apparent center of the shell.

The position of the center of G7.5–1.7 suggests it is the birth remnant of Taz. While the overall X-ray absorption of Taz is significantly higher ( $n_H \sim 1.8 \times 10^{22} \text{ cm}^{-2}$ , RRK) it is also moving into or

behind the Lynds 227 dark cloud. *XMM-Newton* imaging shows some parts of the X-ray nebula are absorbed more than others (Roberts et al. 2006), and a preliminary spectral analysis suggests a range of  $n_H \sim 0.7 - 2.0 \times 10^{22} \text{ cm}^{-2}$ . If we assume Taz and G7.5–1.7 are associated, then the distance to Lynds 227 of 1.7 kpc (Oka et al. 1999) can be considered a lower limit to G7.5–1.7.

From the above estimates of the center of the radio shell, and the pulsar wind nebula line of symmetry, we estimate the birthsite of Taz to be  $l \sim 7.53^\circ$ ,  $b \sim -1.68^\circ$ . The average transverse space velocity is then implied to be  $v_T \sim 200(d_{1.7}/t_{50}) \text{ km s}^{-1}$ , fairly typical for an isolated pulsar. Here  $d_{1.7}$  is the distance in units of 1.7 kpc and  $t_{50}$  is the age in units of 50 kyr. The distance from this estimated birthsite to the pulsar is about half the average distance to the shell ( $R_b \sim 0.62^\circ$ ), which is roughly where a bowshock is expected to begin forming around a pulsar moving within a decelerating SNR shell (van der Swaluw et al. 2004).

If we accept the association with the pulsar and hence the distance to Lynds 227 as a lower limit on the SNR distance, and we further assume it has been undergoing Sedov expansion for the majority of its existence (i.e.  $R \propto t^{0.4}$ ) then we can estimate the current expansion velocity of the shell to be  $v_s \sim 150(d_{1.7}/t_{50}) \text{ km s}^{-1}$ . Note that if the SNR were considerably younger (eg.  $t \lesssim 15,000$  yr), or considerably further away ( $d \gtrsim 5$  kpc), then the velocity of the radio shell would be similar to very young SNRs. For example, only a few degrees away on the sky is the X-ray and radio bright shell of the  $\sim 2000$ yr old Type II remnant SNR G11.2–0.3 which has a well measured expansion velocity of  $\sim 700 \text{ km s}^{-1}$  at a distance of  $\sim 5$  kpc (Roberts et al. 2003; Tam & Roberts 2003). For strong shocks, the temperature behind the shock, which in the case of G11.2–0.3 is  $kT \sim 0.6 \text{ keV}$ , is proportional to the square of the shock velocity. Although the flux from such a shock depends somewhat on the density and composition of the ISM as well as the equilibrium state of the electrons with the ions, such a hot shock would be difficult to hide from ROSAT given the rather bright radio emission and overall low absorption. However, at the estimated velocity of  $\sim 150 \text{ km/s}$  given our nominal distance and age, the bulk of the shock emission would be emitted well below 1 keV where absorption is more impor-

tant and ROSAT is much less sensitive. Therefore, the lack of bright X-ray emission associated with the radio shell is consistent with the interpretation of G7.5–1.7 being at a distance of  $\sim 2$  kpc and an age similar to other mixed-morphology SNR.

G7.5–1.7 is now the fifth known mixed-morphology supernova remnant that is coincident with the error box of one of the 25 brightest sources of GeV emission in our Galaxy, and the fourth of these to contain a pulsar wind nebula. Two of these SNRs also contain known TeV sources, and several other PWN associated with bright GeV sources have TeV emission (Funk et al. 2007), so it is quite plausible that Taz/G7.5–1.7 also has TeV emission. However, in no currently known case is the GeV emission convincingly arising from the same spatial location as the TeV emission. This suggests that GeV and TeV emission may have separate sites of acceleration or represent particle populations with very different ages.

As is the case with the PWN in CTA1 and W44, Taz is actually contained within the GeV error box, while the radio shells are outside the error box. In all three of these cases, there is some evidence of moderate variability of the  $\gamma$ -ray emission, with the source containing Taz showing the strongest evidence (Nolan et al. 2003). The W44/PSR B1853+01 system is very similar in that there is clearly an RPWN seen in both radio and X-rays at the edge of the thermal X-ray emitting region. It also has similar X-ray (Kawasaki et al. 2005) and  $\gamma$ -ray properties (RRK). The rapid motion of the pulsars through the clumpy, dense interior of these remnants provides a natural variability mechanism for emission coming from the immediate environment of the pulsar. However, PSR B1853+01 is only moderately energetic with a spin-down power  $\dot{E} = 4.3 \times 10^{35}$  erg s $^{-1}$ . Therefore, if this is where the variable  $\gamma$ -rays from W44 are produced, then it suggests the interaction of a pulsar wind with the unique hot and dense environment of the interior of mixed-morphology remnants may allow for very efficient  $\gamma$ -ray production.

This research has made use of data obtained from the High Energy Astrophysics Science Archive Research Center (HEASARC), provided by NASA’s Goddard Space Flight Center. The National Ra-

dio Astronomy Observatory Very Large Array is a facility of the National Science Foundation operated under cooperative agreement by Associated Universities, Inc. This research made use of data products from the Midcourse Space Experiment, processing of which data was funded by the Ballistic Missile Defense Organization with additional support from NASA Office of Space Science. This research has also made use of the NASA/ IPAC Infrared Science Archive, which is operated by the Jet Propulsion Laboratory, California Institute of Technology, under contract with the National Aeronautics and Space Administration.

*Facilities:* MSX, Effelsberg, ASCA (GIS), VLA, ROSAT (PSPC)

## REFERENCES

- Aharonian, F. & et al. 2005, A&A, 432, L25
- Aharonian, F. et al. 2006a, A&A, 448, L43
- . 2006b, A&A, 456, 245
- . 2006c, ApJ, 636, 777
- Albert, J. et al. 2007, ApJ, 664, L87
- Baring, M. G., Ellison, D. C., Reynolds, S. P., Grenier, I. A., & Goret, P. 1999, ApJ, 513, 311
- Braje, T. M., Romani, R. W., Roberts, M. S. E., & Kawai, N. 2002, ApJ, 565, L91
- Brazier, K. T. S., Reimer, O., Kanbach, G., & Carraminana, A. 1998, MNRAS, 295, 819
- Brogan, C. L., Devine, K. E., Lazio, T. J., Kassim, N. E., Tam, C. R., Briskin, W. F., Dyer, K. K., & Roberts, M. S. E. 2004, AJ, 127, 355
- Brogan, C. L., Gaensler, B. M., Gelfand, J. D., Lazendic, J. S., Lazio, T. J. W., Kassim, N. E., & McClure-Griffiths, N. M. 2005, ApJ, 629, L105
- Brogan, C. L., Gelfand, J. D., Gaensler, B. M., Kassim, N. E., & Lazio, T. J. W. 2006, ApJ, 639, L25
- Cohen, M. & Green, A. J. 2001, MNRAS, 325, 531
- Dickey, J. M. & Lockman, F. J. 1990, Ann. Rev. Astr. Ap., 28, 215

- Doherty, M., Johnston, S., Green, A. J., Roberts, M. S. E., Romani, R. W., Gaensler, B. M., & Crawford, F. 2003, *MNRAS*, 339, 1048
- Esposito, J. A., Hunter, S. D., Kanbach, G., & Sreekumar, P. 1996, *ApJ*, 461, 820
- Funk, S. 2006, 36th COSPAR Scientific Assembly, 36, 120
- Funk, S., Reimer, O., Torres, D. F., & Hinton, J. A. 2007, *ArXiv e-prints*, 710, arXiv:0710.1584
- Gaensler, B. M. & Slane, P. O. 2006, *ARA&A*, 44, 17
- Gotthelf, E. V., Ueda, Y., Fujimoto, R., Kii, T., & Yamaoka, K. 2000, *ApJ*, 543, 417
- Griffith, M. R., Wright, A. E., Burke, B. F., & Ekers, R. D. 1994, *ApJS*, 90, 179
- H. E. S. S. Collaboration: G. Rowell, Brion, E., Reimer, O., Moriguchi, Y., Fukui, Y., Djannati-Ataï, A., & Funk, S. 2007, *ArXiv e-prints*, 710, arXiv:0710.2017
- Halpern, J. P., Gotthelf, E. V., Camilo, F., Helfand, D. J., & Ransom, S. M. 2004, *ApJ*, 612, 398
- Harrus, I. M., Hughes, J. P., & Helfand, D. J. 1996, *ApJ*, 464, L161
- Hartman, R. C. et al. 1999, *ApJS*, 123, 79
- Helfand, D. J., Gotthelf, E. V., Halpern, J. P., Camilo, F., Semler, D. R., Becker, R. H., & White, R. L. 2007, *ApJ*, 665, 1297
- Kaspi, V. M., Roberts, M. S. E., & Harding, A. K. 2006, *Compact stellar X-ray sources*, 279
- Kawasaki, M., Ozaki, M., Nagase, F., Inoue, H., & Petre, R. 2005, *ApJ*, 631, 935
- Lamb, R. C. & Macomb, D. J. 1997, *ApJ*, 488, 872
- Lockman, F. J., Pisano, D. J., & Howard, G. J. 1996, *ApJ*, 472, 173
- Nolan, P. L., Tompkins, W. F., Grenier, I. A., & Michelson, P. F. 2003, *ApJ*, 597, 615
- Oka, T., Kawai, N., Naito, T., Horiuchi, T., Namiki, M., Saito, Y., Romani, R. W., & Kifune, T. 1999, *ApJ*, 526, 764
- Olbert, C. M., Clearfield, C. R., Williams, N. E., Keohane, J. W., & Frail, D. A. 2001, *ApJ*, 554, L205
- Reich, W., Fuerst, E., Haslam, C. G. T., Steffen, P., & Reif, K. 1984, *A&AS*, 58, 197
- Rho, J. & Petre, R. 1998, *ApJ*, 503, L167+
- Roberts, M. S. E., Gotthelf, E. V., Halpern, J. P., Brogan, C. L., & Ransom, S. M. 2006, *ArXiv Astrophysics e-prints*, arXiv:astro-ph/0612631
- Roberts, M. S. E., Romani, R. W., & Kawai, N. 2001a, *ApJS*, 133, 451
- Roberts, M. S. E., Romani, R. W., Kawai, N., Gaensler, B. M., & Johnston, S. 2001b, in *ASSL Vol. 267: The Nature of Unidentified Galactic High-Energy Gamma-Ray Sources*, 135–152
- Roberts, M. S. E., Tam, C. R., Kaspi, V. M., Lyutikov, M., Vasisht, G., Pivovarov, M., Gotthelf, E. V., & Kawai, N. 2003, *ApJ*, 588, 992
- Sturner, S. J. & Dermer, C. D. 1995, *A&A*, 293, L17
- Tam, C., & Roberts, M. S. E. 2003, *ApJ*, 598, L27
- Tanaka, Y., Inoue, H., & Holt, S. S. 1994, *PASJ*, 46, L37
- Tilley, D. A., Balsara, D. S., & Howk, J. C. 2006, *MNRAS*, 371, 1106
- Torres, D. F., Romero, G. E., Dame, T. M., Combi, J. A., & Butt, Y. M. 2003, *Phys. Rep.*, 382, 303
- Trümper, J. 1982, *Advances in Space Research*, 2, 241
- van der Swaluw, E., Downes, T. P., & Keegan, R. 2004, *A&A*, 420, 937
- Weekes, T. C. et al. 1989, *ApJ*, 342, 379
- Yadigaroglu, I.-A. & Romani, R. W. 1997, *ApJ*, 476, 347